# Investigation of metal oxides toward organic dyes decolourisation and environmental remediation



# Investigation of metal oxides toward organic dyes decolourisation and environmental remediation

**ThianKhoon Tan[1,*], PoiSim Khiew[1], WeeSiong Chiu[2] and ChinHua Chia[3]**

[1] Engineering Foundation, Faculty of Engineering, University of Nottingham Malaysia, Jalan Broga, 43500 Semenyih, Selangor Darul Ehsan, Malaysia
[2] Low Dimensional Materials Research Center, Department of Physics, Faculty of Science, Universiti Malaya, 50603 Kuala Lumpur, Malaysia
[3] School of Applied Physics Studies, Faculty of Science & Technology, Universiti Kebangsaan Malaysia, 43600 Bangi, Selangor Darul Ehsan, Malaysia
[*] E-mail: TK.Tan@nottingham.edu.my

**Abstract.** Enormous interest has been focused on metal oxides in its photocatalytic capabilities toward oxidizing organic dyes and environmental remediation. Zinc oxide (ZnO), titanium dioxide ($TiO_2$) and iron oxide ($Fe_3O_4$) have been used as the heterogeneous photocatalysts to photodegrade three organic dyes, which are methylene blue (MB), phenol red (PR) and methyl orange (MO). Series of 3.0 ml dyes samples in aqueous solutions were placed into a UV chamber under UV-C (254 nm) light irradiation. The oxides powder was characterised by XRD, FESEM and TEM analysis, where ZnO nanoparticles was in hexagonal wurtzite crystal structure (SG: $P6_3mc$) with average crystalline size of (91 ± 12) nm and $TiO_2$ nanoparticles was pure anatase of tetragonal crystal structure (SG: $I4/_amd$) with average crystalline size of (117 ± 16) nm. $Fe_3O_4$ nanoparticles was in cubic spinel crystal structure with average crystalline size of (62.1 ± 5.7) nm. The photocatalyst loading (0.5 – 3.5wt%), initial dye concentration (MB: 2 – 12 ppm, PR: 8 – 48 ppm, MO: 12 – 32 ppm) and irradiation duration on the decolourisation of dye samples were examined. Based on time requirement, the photocatalytic decolourisation rate increased with increasing metal oxide loading and decreased with the increasing of the initial dye concentration. The superior photocatalyst was ZnO with a loading of 2.5 wt% followed by $TiO_2$ (3.0 wt%) and least photocatalytic capability was $Fe_3O_4$ (3.0 wt%). On the other hand, the most photostable dye is MO followed by PR and MB.

## 1. Introduction

In general, metal oxides can take a variety of structural geometries together with an electronic structure that can exhibit different characteristics, such as metallic, semiconductor and insulator. Therefore, they have emerged as a very important substance and contribute in many areas of physics, chemistry and materials science. Recently, metal oxides have gained enormous interest in heterogeneous photocatalysis due to its emerging applications toward environmental remediation and organic synthesis (Amini and Ashrafi 2016). Many researchers attempted to study photocatalytic activity of different metal oxides like ZnO, $CeO_2$, $WO_3$, $TiO_2$, $Cu_2O$, $MnO_2$, $Fe_2O_3$, etc. (Ray and Pal 2017).

Both ZnO and $TiO_2$ have been extensively used as photocatalyst which have become a promising environmental remediation technology, water photoelectrolysis and dye-sensitized solar cells, due to

their low cost, environmental friendly, nontoxicity, high chemical stability and excellent degradation for organic pollutants (Amini and Ashrafi 2016). On the other hand, little is known about the use of iron oxide as a photocatalyst. There are numerous conditions determining the effectiveness of this magnetic nanoparticles in wastewater treatment system and a number of studies have demonstrated the success of $Fe_3O_4$ nanoparticles on the removal of heavy metals from contaminated water (Hou, Tian et al. 2015, Kim, Woo et al. 2016). Besides, this magnetic nanoparticle also showed a sustainable treatment process through reusing and still regaining the removal capacity in few treatment cycles (Chiu, Khiew et al. 2010, Salamat, Younesi et al. 2017).

In the present study, the photodegradation of the three type of dyes, namely methylene blue (MB), phenol red (PR) and methyl orange (MO) were investigated and the most optimum amount of loading for the three metal oxides, ZnO, $TiO_2$ and $Fe_3O_4$ nanoparticles photocatalysts, were evaluated. These dyes were chosen as the organic compound since they are complex organic substances which contain a significant amount of various functional groups and are well dissolved in water. MB dye is easy to monitor by simple techniques such as UV-visible spectroscopy at its maximum absorption wavelength (Nogueira, Castro et al. 2014), with its four main peaks at 665, 614, 293 and 247 nm (Kuan and Chan 2012). On the other hand, PR is a weak organic acid and is a typical reversible pH-sensitive dye. Its absorption maximum wavelength is at 435 nm. Finally, MO is a typical azo dye and generally used in the textile industry. Its absorption maximum wavelength, $\lambda_{max}$, at 466.5 nm (Hakamada, Hirashima et al. 2012).

## 2. Materials and Methods

### *2.1. Materials*

Zinc oxide (ZnO, R & M Chemicals, U.K.), titanium dioxide ($TiO_2$, R & M Chemicals, U.K.) and iron oxide ($Fe_3O_4$, Systerm, ChemPur) purchased are of analytical grades and used without any modification. The dyes include methylene blue ($C_{16}H_{18}N_3SCl•3H_2O$; $M_w$=373.90 g/mol), phenol red ($C_{19}H_{14}O_5S$; $M_w$=354.38 g/mol), and methyl orange ($C_{14}H_{14}N_3NaO_3S$; $M_w$=327.33 g/mol were purchased from R & M Chemicals, UK. All the chemical products were used as received without any further purification. The deionised water obtained from Favorit Water Distiller (Favorit Water Still W4L; conductivity of 3-4 $\mu$s/cm and resistivity of 0.25-0.30 MΩ cm) was used to prepare all the aqueous solutions.

### *2.2. Experimental*

All metal oxides nanopowder was characterised by X-ray diffraction (XRD) using Bruker AXS-D8 Advance diffractometer equipped with $CuK_\alpha$ radiation over the scan range $2\theta$ of 10º to 80º at room temperature. The surface and subsurface imaging were conducted by using the field emission scanning electron microscopy (FESEM) from FEI, Quanta 400 SE/SEM, which is also coupled with energy dispersive X-ray analyser (EDX). The morphology of the sample was studied using a LEO 912AB high-resolution transmission electron microscope (TEM) equipped with energy filter. The specific surface area was determined on the basis of BET instrument using Micromeritics ASAP 2020 V3.01 H.

Individual metal oxides powder was premixed with distilled water in beakers and vials to obtain different concentration of the catalysts loading, that is between 0.50 wt% to 3.50 wt%. In addition, the organic dyes, such as MB, PR and MO, were also premixed by adding the weighted dyes powder with distilled water to obtain aqueous solutions of the desired concentration, in the range of 2.00 ppm to 12.0 ppm for MB, 8.00 ppm to 48.0 ppm for PR and 12.0 ppm to 32.0 ppm for MO. After that, 3.00 ml of organic dye solutions were added with 0.20 g (0.20 mL) of premixed photocatalyst of different concentrations. These mixtures were allowed to be in the dark for about 30 minutes and then shifted and placed under UV light irradiation for various durations, with 10 minutes interval, to allow the degradation process to take place. The photocatalytic degradation was carried out in the UV chamber

(Uvitec Cambridge ultraviolet crosslinker, CL-508.G, with 5 of 8 W tube bulbs) equipped with five UV tube each producing light source of 254 nm wavelength, as shown in Figure 1.

After the irradiation, each individual photocatalyst sample was placed into the centrifuge (Kubota Tabletop Centrifuge 2420). A 2 mL aliquot was taken from the solutions to measure the absorption spectra of the dyes. The first aliquot was withdrawn from the solutions right after the dark absorption/desorption equilibrium period to determine the first absorbance spectrum ($A_o$) of the dye, which represents the initial concentration ($C_o$) of the dye. The absorption spectra of the dyes were evaluated using a UV-Visible Spectrophotometer (Varian, Cary 50) detector with scan rate of 120 nm/min for wavelength range from 200 nm to 800 nm. The degradation was studied by observing at the changes of the absorption maximum of the organic dye used.

*2.3. Decolourisation analysis*

The absorbance calibration curve of the dye solution was used as according to Beer-Lambert law (Kelsall, Hamley et al. 2006). Therefore percentage degradation was calculated from the initial and final absorption of the UV-vis experiments as follows:

$$Degradation\ (\%) = \frac{C_o - C}{C_o} \times 100 = \frac{A_o - A}{A_o} \times 100 \qquad (1)$$

where $C_o$ and $C$ are the initial and post-irradiation concentration of the organic dye, respectively, whereas $A_o$ and $A$ are the initial and post-irradiation absorbance of the dye, respectively, as measured by the UV-vis spectrophotometer.

## 3. Results and Discussion

*3.1. XRD analysis*

Figure 2 shows the XRD characterization for ZnO, $TiO_2$ and $Fe_3O_4$ nanoparticles. First diffraction pattern shows all the peaks are consistent with the database in JCPDS file (#79-0208), which are the standard peaks of the ZnO planes with a hexagonal wurtzite crystal structure (SG: $P6_3mc$) (Saravanan, Mansoob Khan et al. 2015). The diffraction pattern also indicates high purity of the nanopowder as there was no other impurity peaks are observed. For the $TiO_2$ nanoparticles, the $2\theta$ values match the characteristic pattern of pure anatase phase of $TiO_2$ tetragonal structure (SG: $I4/_amd$), with no other crystalline byproducts, in agreement with the literatures JCPDS file #21-1272 (Adachi, Jiu et al. 2008, Liu, Chu et al. 2015).

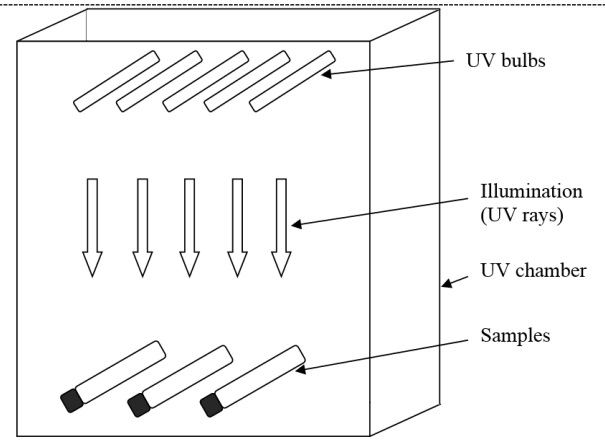


**Figure 1.** Schematic diagram of the experimental set up.

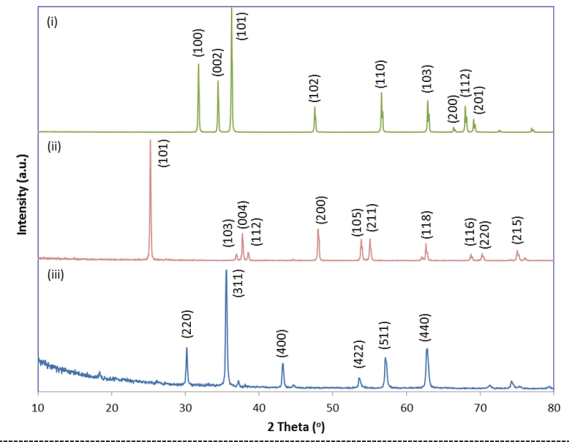


**Figure 2.** X-ray diffraction pattern of (i) ZnO, (ii) $TiO_2$, and (iii) $Fe_3O_4$ nanoparticle photocatalysts.

The XRD diffraction peaks for $Fe_3O_4$ nanoparticles conform to the $Fe_3O_4$ crystal of cubic spinel structure, consistent with literature JCPDS file #19-0629 (Wu, Shen et al. 2011). Its purity, could be supported by the EDX analysis, which was discussed in section 3.5. On top of that, the average crystallite size was evaluated, which are (91 ± 12) nm, (117 ± 16) nm, and (62.1 ± 5.7) nm, for ZnO, $TiO_2$ and $Fe_3O_4$ oxides, respectively.

*3.2. FESEM analysis*

Figures 3, 4 and 5 show the FESEM photos for morphologies of ZnO, $TiO_2$ and $Fe_3O_4$ nanoparticles. All the three oxides show no aggregation with a well disperse nanoparticle. They are fairly homogeneous in size for $TiO_2$ and $Fe_3O_4$, except for ZnO nanoparticles with a slightly wider range of size distribution.

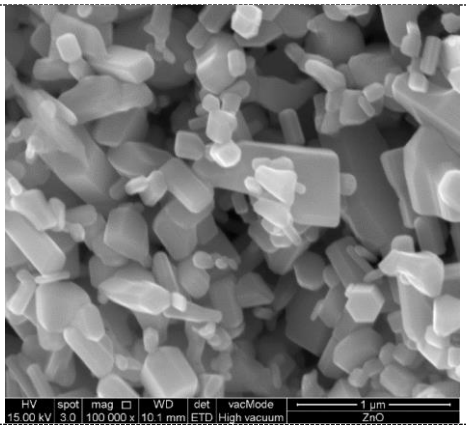


**Figure 3.** FESEM picture of ZnO.

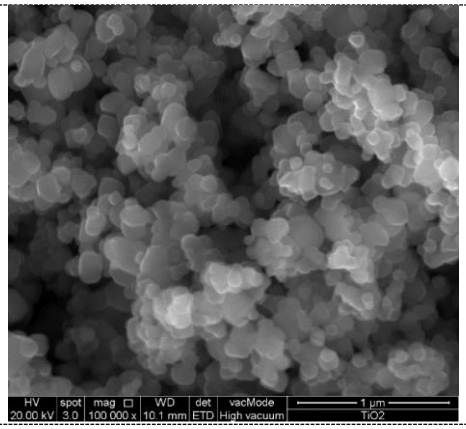


**Figure 4.** FESEM picture of $TiO_2$.

*3.3. TEM analysis*

The ZnO nanoparticles were irregular in shape with spherical to rod-like, as well as particle in blocks. It shows a wide particle size distribution with an average particle size of (93.2 ± 4.6) nm, which was in agreement with the crystallite size obtained from XRD. The $TiO_2$ metal oxide particles were generally spherical with few rod-like shape and fairly monodispersed. The particle size distribution was quite narrow as compared to the other two nanoparticles. The TEM image for the $Fe_3O_4$ nanoparticles was uniformly dispersed throughout with the particles were globular in shape and quite evenly distributed in size, where its average particle size is (64.0 ± 4.6) nm.

*3.4. BET analysis*

The BET measurement for the metal oxides nanoparticles was given in Table 1. The results clearly show that ZnO nanoparticles were having smaller surface area and pore volume if compared to the $TiO_2$ photocatalyst, which might impact its photodegradation capability.

**Table 1.** BET data for ZnO, $TiO_2$ and $Fe_3O_4$ nanoparticles.

| Measurement Properties | ZnO | $TiO_2$ | $Fe_3O_4$ |
|---|---|---|---|
| BET surface area ($m^2/g$) | 2.406 | 6.795 | 12.458 |
| Pore volume ($cm^3/g$) | 0.009720 | 0.04519 | 0.04367 |
| Average pore size (nm) | 16.156 | 26.606 | 14.023 |

*3.5. Energy Dispersive X-ray Spectroscopy (EDX) analysis*

The atomic fraction of each materials elements, ZnO, $TiO_2$ and $Fe_3O_4$, were in close agreement with their chemical formulae, with the values (1:1.12), (1:2.96) and (1:1.52), respectively. The presence of each element for each respective spectrums strengthen the arguments on the purities of these nanoparticles (Hafez, Lan et al. 2010). Together with the XRD analysis, it conforms that the samples are pure, single phase and nanocrystalline in nature.

*3.6. The effects of photocatalysts loading on photocatalytic decolourisation*

There have been many studies being focused on the effects of photocatalyst loading on the photocatalytic degradation of organic dyes in wastewaters (Sugiyana, Handajani et al. 2014, Regulska, Brus et al. 2016). The loading of the metal oxides photocatalysts was varied from 0.50 to 3.50 wt% in increment of 0.50 wt% with the sample dye used was 12.0 ppm MB.

*3.6.1. ZnO photocatalyst.* First-order kinetics study could easily convey the information of rate of the organic substance being degraded (Xie, Wang et al. 2011). The first-order kinetics results for the ZnO photocatalyst can be observed in Figure 6. It is obvious that the degradation rate was lowest for solution without catalyst, at 0.0080 $min^{-1}$. The degradation rate immediately improved with the addition of the ZnO photocatalyst, as the catalyst provides active radicals as well as interaction sites on its surface (Xu, Zhang et al. 2011). It increased until 2.5 wt% (0.2221 $min^{-1}$) of the catalyst loading, but dropped slightly with 3.0 wt% (0.2180 $min^{-1}$) and further decreased to 0.1856 $min^{-1}$ for 3.5 wt% loading. With the increased of the photocatalyst loading, the number of active sites increases. Further increases beyond the optimum level will block the photon light from reaching the other photocatalyst (Velmurugan and Swaminathan 2011).

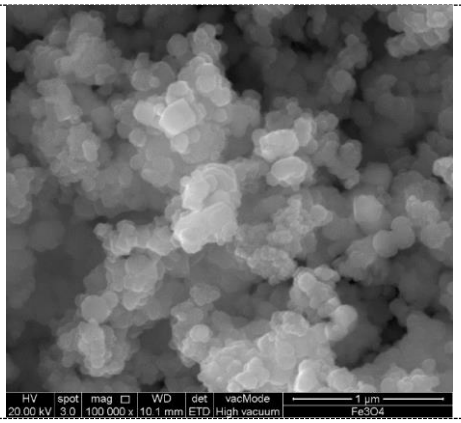


**Figure 5.** FESEM picture of $Fe_3O_4$.

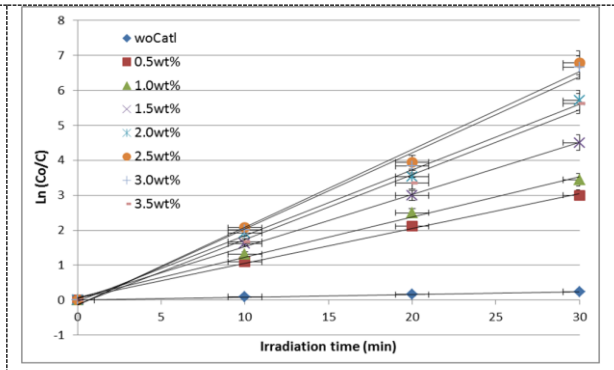


**Figure 6.** First-order kinetics of MB with ZnO photocatalyst.

*3.6.2. $TiO_2$ photocatalyst.* For the $TiO_2$ photocatalyst, as seen in Figure 7, similar pattern of degradation rate was observed. The degradation rate was lowest (0.0051 $min^{-1}$) when no catalyst was added and the degradation rates increased significantly (0.0487 $min^{-1}$ for 0.50 wt% loading) when the $TiO_2$ photocatalyst was present in the solutions. The optimum loading for $TiO_2$ photocatalyst was achieved at 3.0 wt% (0.1012 $min^{-1}$) with a slight dropped in photodegradation rate when the loading was increased to 3.5 wt% (0.0976 $min^{-1}$).

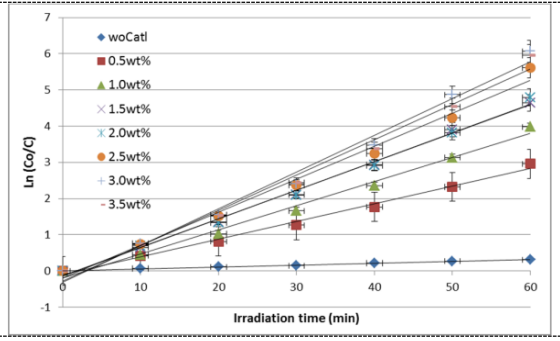


**Figure 7.** First-order kinetics of MB with $TiO_2$ photocatalyst.

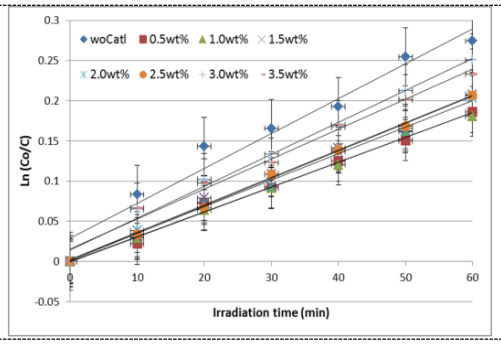


**Figure 8.** First-order kinetics of MB with $Fe_3O_4$ photocatalyst.

*3.6.3. $Fe_3O_4$ photocatalyst.* This metal oxide did not show any photocatalytic capability if compared to the other two photocatalysts, as shown in Figure 8. It is clearly seen that the highest degradation rate was without photocatalyst (0.0043 $min^{-1}$), where the highest degradation was only (0.0040 $min^{-1}$) for 3.0 wt% of $Fe_3O_4$ loading. It is very apparent that $Fe_3O_4$ nanoparticles do not exhibit any photocatalytic capability that able to enhance the photodegradation process. This is in agreement with a report by Singh and his co-researchers on $Fe_3O_4$ which found that $Fe_3O_4$ nanoparticles has insignificant photocatalytic capability. Nonetheless, $Fe_3O_4$ nanoparticles was generally used as a composite material with other photocatalyst materials, such as ZnO, $TiO_2$ etc., due to its magnetic capabilities (Singh, Barick et al. 2013).

*3.7. The effects of initial dye concentration on decolourisation*
In investigating this effect, the samples of dyes used were methylene blue (MB), phenol red (PR) and methyl orange (MO). The photocatalyst loading for ZnO, $TiO_2$ and $Fe_3O_4$ were 2.5, 3.0 and 3.0 wt% respectively.

*3.7.1. Methylene blue.* The concentration of the MB was ranging from 2.00 to 12.0 ppm. The kinetic constant are highest for the lowest dye concentration, especially for the outstanding photocatalyst of the ZnO nanoparticles which shows the steepest slopes. Although the amount of loading for ZnO is slightly less than $TiO_2$ and $Fe_3O_4$ nanoparticles, it might be due to the ability of the ZnO nanoparticles to absorb more light quanta than $TiO_2$ (Gupta, Saurava et al. 2015). The kinetic constant values of ZnO, $TiO_2$ and $Fe_3O_4$ photocatalysts are recorded as 1.2160 ($R^2$ = 1.0000), 0.2582 ($R^2$ = 0.9929) and 0.0237 $min^{-1}$ ($R^2$ = 0.9963), respectively for 2.00 ppm MB.

*3.7.2. Phenol red.* The result shows that the degradation rates decreased with the increases of the PR dye concentration, especially for the ZnO and $TiO_2$ photocatalysts. However, when the concentration was higher, the degradation rate gradually decreases due to the competition between the contaminant with the hydroxyl ions to be absorbed on the active site of the photocatalyst surface. On the other hand, the degradation rate for the $Fe_3O_4$ photocatalyst was stagnant for all the concentrations.

*3.7.3. Methyl orange.* Both ZnO and $TiO_2$ photocatalysts show very obvious changes of the degradation rates, started with highest degradation rate for the lowest concentration (12.0 ppm) with 0.0868 $min^{-1}$, $R^2$ = 0.9427 for ZnO and 0.0103 $min^{-1}$, $R^2$ = 0.9925 for $TiO_2$. Subsequently, with the increased of the MO concentration, it leads to the distortion of degradation efficiency. The first-order kinetics for the $Fe_3O_4$ photocatalyst shows an inconsistent degradation rate with even a negative value for one of the concentration. This was due to the very small changes on the measurements across the irradiation duration; indicating no degradation took place, as MO is an azo and very stable dye (Hakamada, Hirashima et al. 2012).

## 4. Conclusion

From this study, all the oxide nanoparticles used were of standard crystal structures and well dispersed. There were no impurities observed during the characterization of the nanoparticles. By using MB as a model dye, optimum photocatalyst loadings for the three photocatalysts were obtained. It was found that the optimum loading for ZnO was 2.5wt%, whereas for $TiO_2$ and $Fe_3O_4$ was 3.0wt%. MB was completely decomposed between 10 to 20 minutes of irradiation duration in the presence of ZnO photocatalyst, whereas for $TiO_2$ photocatalyst, MB was decomposed in between 20 to 30 minutes of irradiation. Nonetheless, $Fe_3O_4$ photocatalyst was just able to decomposed 72.8% of the MB in 60 minutes of irradiation. For the decomposition of PR, ZnO and $TiO_2$ photocatalysts were able to degrade PR solutions within 30 and 50 minutes of irradiation, respectively. However, $Fe_3O_4$ showed only very mild decomposition even after 60 minutes of irradiation. In the photodecomposition of MO, it was completely decomposed by ZnO in 50 minutes of irradiation, whereas $TiO_2$ decomposed 45.9% of MO in 60 minutes of irradiation. On the other hand, no trace of decomposition could be detected for the 60 minutes irradiation with the presence of $Fe_3O_4$ nanoparticles. It can be concluded that ZnO is the superior photocatalyst followed by $TiO_2$, whereas $Fe_3O_4$ showed very mild photocatalytic capability. In term of photostability of the dyes, it showed that MO is the most stable dye followed by PR and MB. This result was consistent for all the dyes whether they are irradiated under UV light irradiation with or without the presence of photocatalysts.

**Acknowledgments**
We are greatly acknowledged the financial support obtained from MOSTI, Government of Malaysia, with the grant No. 03-02-12-SF0019.

**5. References**

[1] Adachi, M, Jiu, J, Isoda, S, Mori, Y, and Uchida, F 2008 *Nanotechnol. Sci. Appl.* **1** 1-7
[2] Amini, M, and Ashrafi, M 2016 *Nano. Chem. Res.* **1**(1) 79-86
[3] Chiu, W S et al. 2010 *Chemical Engineering Journal* **158**(2) 345-352
[4] Gupta, A, Saurava, J R, and Bhattacharya, S 2015 *RSC Adv.* **5** 71472-71481
[5] Hafez, H, Lan, Z, Li, Q, and Wu, J 2010 *Nanotechnol Sci Appl.* **3** 45–51
[6] Hakamada, M, Hirashima, F, and Mabuchi, M 2012 *Catalysis Science & Technology* **2**(9) 1814
[7] Hou, X, Tian, Y, Zhang, X, Dou, S, Pan, L, Wang, W, Li Y, and Zhao, J 2015 *Journal of Alloys and Compounds, 638*, 214-220
[8] Kelsall, R, Hamley, I, and Geoghegan, M 2006 *Nanoscale Science and Technology* West Sussex, England: John Wiley and Sons Ltd
[9] Kim, S -E, Woo, J -Y, Kang, S -Y, Min, B K, Lee, J K, and Lee, S -W 2016 *Journal of Industrial and Engineering Chemistry* **43** 142–149
[10] Kuan, W -H, and Chan, Y -C 2012 *Journal of Hazardous Materials* **239-240** 152-159
[11] Liu, S, Chu, J, Guo, X, Ge, J, and Wu, H 2015 *Colloids and Surfaces A: Physicochemical and Engineering Aspects* **484** 434-440
[12] Nogueira, A E, Castro, I A, Giroto, A S, and Magriotis, Z M 2014 *Journal of Catalysts* **2014** 712067
[13] Ray, C and Pal, T 2017 *J. Mater. Chem. A* **5** 9465
[14] Regulska, E, Brus, D M, Rodziewicz, P, Sawicka, S, and Karpinska, J 2016 *Catalysis Today* **266** 72-81 doi:10.1016/j.cattod.2015.08.010
[15] Salamat, S, Younesi, H and Bahramifar, N 2017 *RSC Adv.* **7** 19391
[16] Saravanan, R, Mansoob Khan, M, Gupta, V K, Mosquera, E, Gracia, F, Narayanan, V, and Stephen, A 2015 *Journal of Colloid and Interface Science* **452** 126–133
[17] Singh, S, Barick, K C, and Bahadur, D 2013 *Journal of Materials Chemistry A* **1**(10) 3325
[18] Sugiyana, D, Handajani, M, Kardena, E, and Notodarmojo, S 2014 *Journal of JSCE* **2** 69-76
[19] Velmurugan, R, and Swaminathan, M 2011 *Solar Energy Materials and Solar Cells* **95**(3) 942-950 doi:10.1016/j.solmat.2010.11.029
[20] Wu, C, Shen, L, Zhang, Y -C, and Huang, Q 2011 *Materials Letters* **65**(12) 1794-1796
[21] Xie, J, Wang, H, Duan, M, and Zhang, L 2011 *Applied Surface Science* **257**(15) 6358-6363
[22] Xu, T, Zhang, L, Cheng, H, and Zhu, Y 2011 *Applied Catalysis B: Environmental* **101**(3-4) 382-387 doi:10.1016/j.apcatb.2010.10.007